Relative Formation Rate Constants and Electronic-State Distribution of Ne* Produced from the Ne^+/2e^- Collisional Radiative Recombination in the He Flowing Afterglow

TSUJI, Masaharu
Institute for Materials Chemistry and Engineering, and Research and Education Center of Green Technology, Kyushu University

HISANO, Masahiro
Department of Applied Science for Electronics and Materials, Kyushu University : Graduate Student

UTO, Keiko
Institute for Materials Chemistry and Engineering, and Research and Education Center of Green Technology, Kyushu University

HAYASHI, Jun-Ichiro
Institute for Materials Chemistry and Engineering, and Research and Education Center of Green Technology, Kyuhu University

他

https://doi.org/10.15017/5208233

出版情報：九州大学大学院総合理工学報告. 44 (2), pp.1-8, 2023-02. 九州大学大学院総合理工学府
バージョン：
権利関係：

九州大学大学院総合理工学府報告
第 44 巻 第 2 号 1-8 頁 令和 5 年 2 月

Engineering Sciences Reports, Kyushu University
Vol. 44, No. 2, pp. 1-8, FEB, 2023

Relative Formation Rate Constants and Electronic-State Distribution of Ne* Produced from the $Ne^+/2e^-$ Collisional Radiative Recombination in the He Flowing Afterglow

Masaharu TSUJI*1,2† Masahiro HISANO*3 Keiko UTO*1
Jun-Ichiro HAYASHI*1 Takeshi TSUJI*4
†E-mail of corresponding author: tsuji@cm.kyushu-u.ac.jp

(Received October 31, 2022, accepted November 10, 2022)

Relative formation rate constants, $k_0(u)$, and the electronic-state distribution, $N(u)$, of Ne* for upper u states were determined in the $Ne^+/2e^-$ collisional radiative recombination (CRR) by observing Ne* atomic emissions in the 200–990 nm region. To exclude the contribution of Ne_2^+/e^- dissociative recombination (DR), He flowing afterglow was used, where only atomic Ne^+ ions were generated by the He_2^+/Ne charge-transfer reaction. Sixty-eight *ns*(*n*=4–7), *ns*′(*n*=4 and 5), *np*(*n*=3 and 4), *np*′(*n*=3 and 4), *nd*(*n*=3–7, 9–11), and *nd*′(*n*=3–6) levels of Ne* were identified. Major product Ne* states ($\sum_u k_0(u)$ and $\sum_u N(u)$) excluding radiative cascade were 4*s*, 4*s*′, 3*d*, 3*d*′, and 5*d* states, which occupied 16.1, 60.6, 12.8, 5.6, and 2.7% of $\sum_u k_0(u)$ and 17.0, 40.3, 13.1, 6.0, and 18.5% of $\sum_u N(u)$, respectively. The electronic-state distribution of Ne* in the 19.66–21.11 eV range increased with decreasing the excitation energy of Ne*. Using a Saha equation for CRR, it was expressed by a single Boltzmann distribution with an effective electronic temperature of 0.43 eV. This value was close to that of He* in the $He^+/2e^-$ CRR (0.46 eV), whereas it was lower than that of Ar* in the $Ar^+/2e^-$ CRR (0.54 eV).

Key words: *Atomic neon ion, Collisional radiative recombination, Flowing afterglow, Ne* emission, Relative formation rate constant, Electronic-state distribution, Radiative cascade, Saha equation, Boltzmann temperature*

1. Introduction

Electron–ion recombination in ionized gases can occur through dissociative recombination (DR) and collisional radiative recombination (CRR). DR is the fastest recombination process whenever molecular ions are the dominant ionic species.

$$AB^+ + e^- \rightarrow A + B \qquad (1)$$

When dominant ionic species are atomic ions, collisional radiative recombination (CRR) becomes the principal loss process of free electrons.

$$A^+ + e^- + e^- \rightarrow A + e^- \qquad (2)$$

The importance of CRR processes in electrical discharges and astrophysical plasmas has motivated extensive theoretical and experimental studies on CRR. Although rate constants of CRR have been determined theoretically and experimentally,[1-6] little experimental studies have been carried out on the product electronic-state distributions.

We have previously studied $He^+/2e^-$ and $Ar^+/2e^-$ CRR reactions by observing He* and Ar* emissions in the flowing afterglow.[7-9] In the $He^+/2e^-$ CRR reaction, the formation of fifty-one singlet and triplet *ns*, *np*, and *nd* Rydberg states of He* in the 23.01–24.53 eV range was observed. The electronic-state distribution decreased with increasing the excitation energy

*1 Institute for Materials Chemistry and Engineering, and Research and Education Center of Green Technology
*2 Department of Applied Science for Electronics and Materials
*3 Department of Applied Science for Electronics and Materials, Graduate Student
*4 Department of Materials Science, Shimane University

of He*. They were expressed by double Boltzmann electronic distributions with effective electronic temperatures of 0.46 eV in the 22.7–24.4 eV range and 0.089 eV in the 24.4–24.5 eV range.

In the $Ar^+/2e^-$ CRR reaction, the $Ar^+(^2P_{3/2})$ spin–orbit component was selected by using a filter gas of the $Ar^+(^2P_{1/2})$ component. Spectral analysis indicated that thirty-four Ar*(4*p*, 4*d*, 5*p*, 5*d*, 6*s*, 6*p*, 6*d*, 4*p′*, 4*d′*, 5*p′*, 5*d′*, and 6*s′*) states in the 13.08–15.33 eV range were produced. Their electronic-state distribution decreased with an increase in the excitation energy of Ar*, which was expressed by a Boltzmann electronic temperature of 0.54 eV. It was concluded that the 4*p* and 4*p′* states were dominantly formed via two-electron process, while most of the 4*d*, 5*p*, 5*d*, 6*s*, 6*p*, and 6*d* states were produced via one-electron process.

Optical spectroscopic studies on the Ne_2^+/e^- DR (3) and $Ne^+/2e^-$ CRR (4), on which the present work focuses, have been carried out by Sauter et al.[10] and Gordeev et al.[11]

$$Ne_2^+ + e^- \rightarrow Ne^* + Ne \qquad \text{(DR)} \qquad (3)$$

$$Ne^+ + e^- + e^- \rightarrow Ne^* + e^- \qquad \text{(CRR)} \qquad (4)$$

Sauter et al. measured the time dependence of the intensities of spectral lines and that of the number density of atomic and molecular ions in decaying plasmas produced in neon and helium-neon mixtures.[10] They found that 2*p* and 3*p* levels were produced though DR (3), whereas 4*d* levels were formed by CRR (4). Gordeev et al.[11] studied above DR and CRR processes by using a kinetic spectroscopy method. They used the afterglow of a neon plasma generated by a barrier discharge at neon pressures of 0.2–152 Torr (1 Torr = 133.3 Pa) and electron densities $[e^-] \leq 5 \times 10^{10}$ cm^{-3}. They reported that lower six 4*p* levels were formed by DR of molecular ions with electrons based on a comparison of the dependences of the intensities of spectral lines on time in the afterglow and their response to pulsed "heating" of the electrons. The dominant role in the population of all levels of the $2p^5 4p$ configuration belonged to the CRR of Ne^+ ions at the minimum pressure of 0.33–0.2 Torr.

To the best of our knowledge, no study on the relative formation rate constants and the electronic-state distribution of Ne* in the $Ne^+/2e^-$ CRR process has been carried out at thermal energy. In this study, the $Ne^+/2e^-$ CRR reaction is investigated by observing ultraviolet-visible-near infrared emissions of Ne* in the He flowing afterglow. The relative formation rate constants and electronic-state distribution are determined and discussed in terms of Saha equilibrium. The observed effective Boltzmann temperature is compared with our previous data for $He^+/2e^-$ and $Ar^+/2e^-$ CRR reactions.[8,9]

2. Experimental

We have previously made optical spectroscopic studies on reactions of Ne active species with simple molecules by using Ne afterglow apparatus.[12-15] It was found that metastable $Ne(^3P_{0,2})$ atoms are major active species at low Ne buffer gas pressure below about 0.2 Torr, whereas not only $Ne(^3P_{0,2})$ atoms but also Ne^+ and Ne_2^+ ions exist as active species above that. The $[Ne_2^+]/[Ne^+]$ ratio increased with increasing the Ne gas pressure because Ne_2^+ ions are formed by the $Ne^+/2Ne$ termocular reaction.[16]

$$Ne^+ + Ne + Ne \rightarrow Ne_2^+ + Ne \qquad (5)$$
$$k_5 = (4.4 \pm 0.4) \times 10^{-32} \text{ cm}^6 \text{ s}^{-1}$$

When we use Ne flowing afterglow, both DR (3) and CRR (4) can participate in the formation of Ne* atoms. It was difficult to separate above two recombination processes completely in the Ne afterglow. To isolate CRR reaction (4), we used here He afterglow reaction of Ne. In a He flowing afterglow, such He active species as $He(2^3S)$, He^+, and He_2^+ were initially generated by a microwave discharge of high purity He gas (>99.9999%) at a microwave power of 100 W.[15] The contribution of such charged species as He^+, He_2^+, and electrons to the observed emissions was examined by using a charged-particle collector grid placed between the discharge section and the reaction zone. A small amount of Ne gas (26 mTorr) was added 10 cm downstream from the center of discharge. We used a low partial Ne pressure to suppress the formation of Ne_2^+ by the termolecular reactions (5) and (6).

$$Ne^+ + Ne + He \rightarrow Ne_2^+ + He \qquad (6)$$

The booster pump used in the present apparatus was equipped with a continuously variable gate valve. Opening or closing the gate valve allowed us to vary the flow tube pressure from 1 Torr to 18 Torr.

By the reactions of $He(2^3S)$, He^+, and He_2^+ with Ne, the following primary reactions occur near the Ne gas inlet.[12,17,18]

$$He(2^3S) + Ne \rightarrow Ne^*(4s,4s') + He \quad (7)$$
$$k_7 = 3.85 \times 10^{-12}\ cm^3\ s^{-1}$$

$$He^+ + Ne \rightarrow Ne^+ + He \quad (0.87) \quad (8a)$$
$$\rightarrow HeNe^+ + h\nu\ (0.17) \quad (8b)$$
$$k_{8a} = (1.20 \times 10^{-15}) \pm 30\%\ cm^3\ s^{-1}$$

$$He_2^+ + Ne \rightarrow Ne^+ + 2He \quad (9)$$
$$k_9 = (6.00 \times 10^{-10}) \pm 30\%\ cm^3\ s^{-1}$$

It should be noted that the rate constant of reaction (9) is larger than that of (8) by five orders of magnitude. It is therefore reasonable to assume that Ne^+ atomic ions formed by reaction (9) are dominant ionic species in our experimental condition.

In our He afterglow reaction of Ne, excited Ne* states can be formed by energy transfer reaction (7) and CRR reaction (4). Without applying an electrostatic potential to the charged-particle collector grids, Ne* lines resulting from both reactions (7) and (4) are observed, whereas those resulting only from reaction (4) are obtained by applying an electrostatic static potential to grids. Thus, the Ne* lines resulting only from CRR reaction (4) are obtained by subtracting the contribution of energy-transfer reaction (7). There are two spin-orbit components $^2P_{3/2}$ and $^2P_{1/2}$ in the ground state of Ne^+ with recombination energies of 21.56 and 21.66 eV, respectively, although their relative concentration is not estimated in this study.

A reaction flame, observed 10 cm downstream from the inlet of Ne gas, was dispersed in the 200–990 nm ranges with a Spex 1250M monochromator in the first order of 1200 grooves/mm gratings blazed at 300 nm or 500 nm. Cooled photomultipliers (Hamamatsu Photonics R376 and R316-02) were used for the measurements in the 200–830 nm and 600–990 nm, respectively. The monochromator and the optical detection system were corrected by using standard D_2 and halogen lamps. All spectra presented here were corrected for the wavelength response of the detection system.

3. Results and Discussion

3.1 Emission spectra of Ne* lines resulting from the $Ne^+/2e^-$ CRR reaction

Figures 1(a) and 2(a) show typical emission spectra observed in the 300–900 nm region at a He gas pressure of 18 Torr, where Ne* emissions from the *ns, ns', np, np',* and *nd*

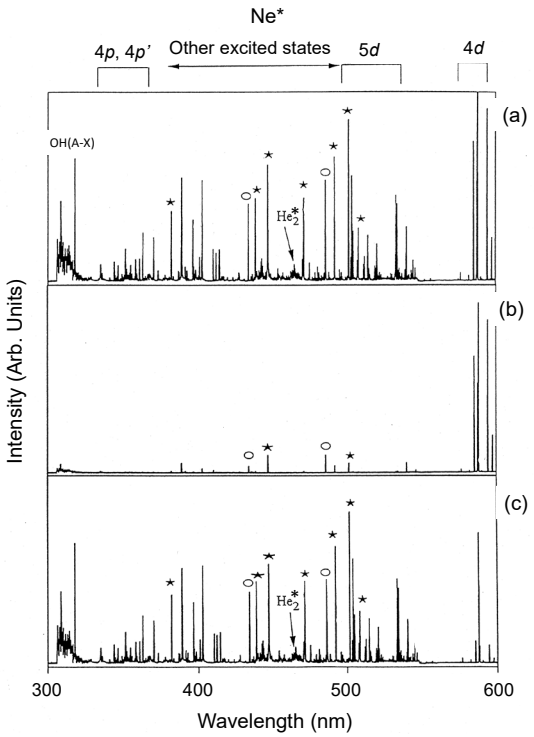

Fig. 1. Emission spectra resulting from (a) $He(2^3S)/Ne + Ne^+/2e^-$, (b) $He(2^3S)/Ne$, and (c) $Ne^+/2e^-$ reactions in the 300–600 nm region. Lines marked by * and o are He* and H* lines, respectively.

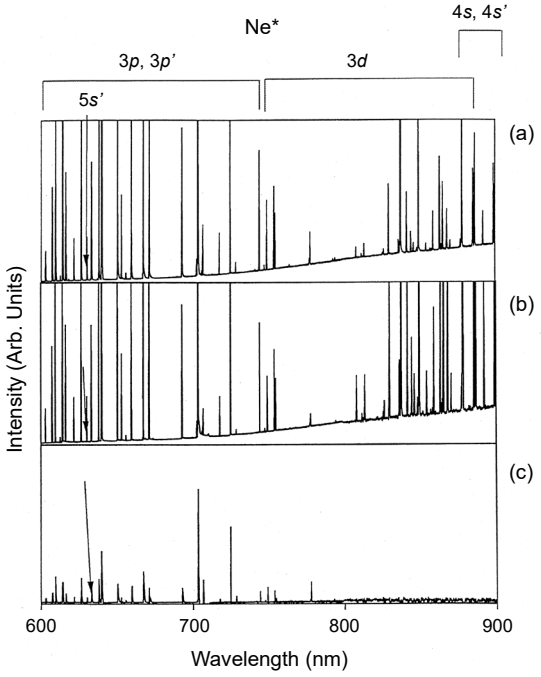

Fig. 2. Emission spectra resulting from (a) $He(2^3S)/Ne + Ne^+/2e^-$, (b) $He(2^3S)/Ne$, and (c) $Ne^+/2e^-$ reactions in the 600–900 nm region.

Rydberg states are identified. In addition, He*, H*, He_2(e-a),[19] and OH(A-X) emissions are observed. H* and OH(A-X) emissions arise from residual H_2O as impurity bands.[20] The observed Ne* lines either disappeared or became very weak when charged species were removed from the He afterglow on applying an electrostatic potential to the grid, as shown in Figs. 1(b) and 2(b). A similar disappearance or a great reduction of the Ne* lines occurred when thermal electrons in the He afterglow were removed by the addition of a small amount of a thermal-electron scavenger (CCl_4) to the reaction zone. These results imply that the Ne* states are produced through electron-ion recombination process.

Emission spectra resulting from the $Ne^+/2e^-$ CRR reaction are obtained by subtracting spectra (b) from spectra (a), and results obtained are shown in Figs. 1(c) and 2(c). The upper electronic states of the observed Ne* transitions in the 260–990 nm region and their excitation energies are listed in Table 1. The spectral assignment was made by referring to reported atomic spectral tables,[21,22] and the excitation energies of Ne* were obtained from reported tables.[22,23] In the present study, 148 Ne* lines from the total 68 *ns*(*n*=4–7), *ns'*(*n*=4 and 5), *np*(*n*=3 and 4), *np'*(*n*=3 and 4), *nd*(*n*=3–7, 9–11), and *nd'*(*n*=3–6) levels are identified with excitation energies of 18.38–21.45 eV. Since the recombination energy of $Ne^+(^2P_{3/2})$ is 21.559 eV, the energies of the observed Ne* states are 0.11–3.18 eV below the ground state of $Ne^+(^2P_{3/2})$. In Table 1, *nL* and *nL'* states of Ne* have $2p^5(^2P_{3/2})nL$ and $2p^5(^2P_{1/2})nL'$ (*n*=3–11, *L*=*s*, *p*, *d*) electron configurations, respectively. The formation of *nL* and *nL'* states of Ne* as product states implies that Ne* states having both $Ne^+(^2P_{3/2})$ and $Ne^+(^2P_{1/2})$ ion-core are produced in the $Ne^+/2e^-$ CRR reaction.

3.2 Relative formation rate constants and electronic-state distribution of Ne* in the $Ne^+/2e^-$ CRR reaction

The formation rate constant of an upper Ne* state, $k(u)$, and its steady-state electronic-state distribution, $N(u)$, in the $Ne^+/2e^-$ CRR reaction were evaluated from the emission intensity of a (u,l) transition of Ne*, I_{ul}, using the following relation:

$$k(u) \propto \sum_l I_{ul} = N(u) \sum_l A_{ul} \qquad (10)$$

Here, A_{ul} is the Einstein coefficient for spontaneous emission, which has been reported previously for most transitions observed here.[22] The overall rate of production of Ne*(u) directly and by cascade from higher excited levels h is given by

$$[\mathrm{Ne}*(u)]/dt = k(u)[\mathrm{Ne}^+][\mathrm{e}^-]^2 = k_0(u)[\mathrm{Ne}^+][\mathrm{e}^-]^2 + \sum_h b_{hu}\, k(h)[\mathrm{Ne}^+][\mathrm{e}^-]^2 \qquad (11)$$

where b_{hu} is the optical branching ratio for the $h \rightarrow u$ transition:

$$b_{hu} = A_{hu}\left(\sum_j A_{hj}\right)^{-1}. \qquad (12)$$

Equation (11) gives

$$k(u) = k_0(u) + \sum_h b_{hu}\, k(h) = k_0(u) + k(u\text{: cascade}). \qquad (13)$$

The rate constant for the direct excitation of a u level, $k_0(u)$, is deduced from Eq. (13), and the corresponding population, $N(u)$, is calculated from the relation:

$$N(u) \propto k_0(u) / \sum_l A_{ul} \qquad (14)$$

In Table 1 and Figs. 3(a) and 3(b) are given $k(u)$, $k(u\text{: cascade})$, and $k_0(u)$ values obtained from total intensities of observed emission lines and unobserved lines. Intensities of unobserved lines were estimated from reported A_{ul} values for Ne* levels in the 18.37–21.11 eV region.[22] No significant differences in $k(u)$ and $k(u\text{: cascade})$ values were observed at total He pressures of 5, 10, 15, and 18 Torr. Therefore, $k(u)$ and $k(u\text{: cascade})$ values given in Table 1 were obtained by averaging four data at different total He pressures. Since the A_{ul} values for Ne* levels in the high energy 21.14–21.45 eV region have not been reported, their $k(u)$ values were evaluated using reported relative intensity of each line.[22] A comparison between $k(u)$ and $k_0(u)$ values suggests that all $3p$ and $3p'$ levels in the 18.37–18.97 eV region and $4p$ and $4p'$ levels in the 20.20–20.30 eV region are formed through radiative cascade from upper levels. On the other hand, both

Table 1. Relative formation rate constants and electronic-state distributions of Ne* produced through the $Ne^+/2e^-$ CRR reaction in the He flowing afterglow.

Energy / eV	State	J	$k(u)$	$k(u:\text{cascade})$	$k_0(u)$	$N(u)$	$\ln(N(u)/g_u)$	ΣA_i (s^{-1}) [a)]
18.38	3*p* [1/2]	1	6.48E-02	6.48E-02	0.00E+00			3.93E+07
18.56	3*p* [5/2]	3	9.99E-02	9.99E-02	0.00E+00			5.15E+07
18.58	3*p* [5/2]	2	1.01E-01	1.01E-01	0.00E+00			4.90E+07
18.61	3*p* [3/2]	1	5.92E-02	5.92E-02	0.00E+00			5.12E+07
18.64	3*p* [3/2]	2	8.47E-02	8.47E-02	0.00E+00			4.98E+07
18.69	3*p′* [3/2]	1	9.48E-02	9.48E-02	0.00E+00			5.08E+07
18.70	3*p′* [3/2]	2	1.23E-01	1.23E-01	0.00E+00			5.27E+07
18.71	3*p* [1/2]	0	1.81E-02	1.81E-02	0.00E+00			6.06E+07
18.73	3*p′* [1/2]	1	8.50E-02	8.50E-02	0.00E+00			5.49E+07
18.97	3*p′* [1/2]	0	1.80E-02	1.80E-02	0.00E+00			6.24E+07
19.66	4*s* [3/2]°	2	7.71E-02	2.12E-04	7.69E-02	3.63E-01	-2.62	2.52E+07
19.69	4*s* [3/2]°	1	2.16E-01	2.38E-04	2.15E-01	2.64E-01	-2.43	9.68E+07
19.76	4*s′* [1/2]°	0	1.02E-01	2.05E-04	1.02E-01	4.81E-01	-0.73	2.52E+07
19.78	4*s′* [1/2]°	1	1.00E+00	4.77E-04	1.00E+00	1.00E+00	-1.10	1.19E+08
20.02	3*d* [1/2]°	0	7.92E-03		7.92E-03	1.75E-02	-4.05	5.38E+07
20.03	3*d* [1/2]°	1	3.33E-02	4.14E-06	3.33E-02	5.14E-02	-4.07	7.71E+07
20.03	3*d* [7/2]°	4	5.14E-02		5.14E-02	1.22E-01	-4.30	4.99E+07
20.03	3*d* [7/2]°	3	3.34E-02	2.26E-07	3.34E-02	8.18E-02	-4.45	4.85E+07
20.04	3*d* [3/2]°	2	2.48E-02	3.66E-07	2.48E-02	5.82E-02	-4.45	5.05E+07
20.04	3*d* [3/2]°	1	3.47E-02		3.47E-02	3.39E-02	-4.48	1.22E+08
20.05	3*d* [5/2]°	2	1.87E-02		1.87E-02	4.76E-02	-4.66	4.66E+07
20.05	3*d* [5/2]°	3	2.78E-02		2.78E-02	7.10E-02	-4.59	4.66E+07
20.14	3*d′* [5/2]°	2	3.08E-02		3.08E-02	7.53E-02	-4.20	4.86E+07
20.14	3*d′* [5/2]°	3	1.99E-02		1.99E-02	4.94E-02	-4.95	4.79E+07
20.14	3*d′* [3/2]°	2	2.52E-02		2.52E-02	6.16E-02	-4.40	4.85E+07
20.14	3*d′* [3/2]°	1	2.52E-02		2.52E-02	3.54E-02	-4.44	8.47E+07
20.20	4*p* [5/2]	2	2.23E-02	2.23E-02	0.00E+00			7.01E+06
20.21	4*p* [3/2]	1	1.27E-03	1.27E-03	0.00E+00			7.77E+06
20.26	4*p* [1/2]	0	4.35E-04	4.35E-04	0.00E+00			1.14E+07
20.29	4*p′* [3/2]	1	6.89E-04	6.89E-04	0.00E+00			7.67E+06
20.30	4*p′* [1/2]	1	1.38E-03	1.38E-03	0.00E+00			8.40E+06
20.30	4*p′* [3/2]	2	1.14E-03	1.14E-03	0.00E+00			7.55E+06
20.56	5*s* [3/2]°	2	1.52E-03		1.52E-03	1.37E-02	-5.90	1.32E+07
20.57	5*s* [3/2]°	1	2.52E-03		2.52E-03	5.77E-03	-6.25	5.20E+07
20.66	5*s′* [1/2]°	0	1.95E-04		1.95E-04	1.78E-03	-6.33	1.30E+07
20.66	5*s′* [1/2]°	1	6.82E-03		6.82E-03	1.97E-02	-5.02	4.10E+07
20.70	4*d* [1/2]°	1	5.37E-03		5.37E-03	9.67E-03	-5.74	6.60E+07
20.71	4*d* [7/2]°	4	1.83E-03		1.83E-03	1.20E-02	-6.62	1.81E+07
20.71	4*d* [7/2]°	3	1.52E-03		1.52E-03	1.04E-02	-6.51	1.73E+07
20.71	4*d* [3/2]°	2	1.35E-03		1.35E-03	8.82E-03	-6.34	1.82E+07
20.71	4*d* [3/2]°	1	2.33E-03		2.33E-03	4.83E-03	-6.43	5.72E+07
20.71	4*d* [5/2]°	2	1.29E-03		1.29E-03	9.04E-03	-6.32	1.69E+07
20.71	4*d* [5/2]°	3	1.14E-03		1.14E-03	7.95E-03	-6.78	1.70E+07
20.80	4*d′* [5/2]°	2	7.76E-04		7.76E-04	5.25E-03	-6.86	1.76E+07
20.80	4*d′* [3/2]°	2	3.08E-03		3.08E-03	2.04E-02	-5.50	1.79E+07
20.81	4*d′* [3/2]°	1	3.09E-03		3.09E-03	8.45E-03	-5.87	4.35E+07
20.94	6*s* [3/2]°	2	9.61E-04		9.61E-04			

Table 1. Continued.

Energy / eV	State	J	$k(u)$	$k(u:\text{cascade})$	$k_0(u)$	$N(u)$	$\ln(N(u)/g_u)$	ΣA_i (s^{-1}) a)
20.95	6*s* [3/2]°	1	2.22E-04		2.22E-04	1.28E-03	-7.76	2.06E+07
21.02	5*d* [7/2]°	3	3.13E-02		3.13E-02	5.75E-01	-2.50	6.48E+06
21.02	5*d* [3/2]°	2	8.34E-04		8.34E-04	1.42E-02	-5.86	6.96E+06
21.02	5*d* [3/2]°	1	1.42E-02		1.42E-02	5.41E-02	-4.02	3.12E+07
21.02	5*d* [5/2]°	2	8.95E-04		8.95E-04	1.67E-02	-5.70	6.36E+06
21.02	5*d* [5/2]°	3	1.16E-03		1.16E-03	2.16E-02	-5.78	6.38E+06
21.11	5*d′* [3/2]°	2	1.51E-03		1.51E-03	2.63E-02	-5.25	6.81E+06
21.11	5*d′* [5/2]°	3	1.01E-03		1.01E-03	1.84E-02	-5.94	6.50E+06
21.14	7*s* [3/2]°	2	1.58E-04		1.58E-04			
21.15	7*s* [3/2]°	1	5.10E-05		5.09E-05			
21.18	6*d* [1/2]°	1	2.60E-04		2.60E-04			
21.19	6*d* [5/2]°	2	1.63E-04		1.63E-04			
21.28	6*d′* [5/2]°	2	3.25E-03		3.25E-03			
21.28	6*d′* [5/2]°	3	4.74E-04		4.74E-04			
21.28	6*d′* [3/2]°	1	1.81E-04		1.81E-04			
21.28	7*d* [1/2]°	1	6.90E-05		6.89E-05			
21.29	7*d* [7/2]°	4	1.24E-04		1.24E-04			
21.29	7*d* [3/2]°	2	2.57E-04		2.57E-04			
21.40	9*d* [7/2]°	4	2.58E-05		2.58E-05			
21.43	10*d* [7/2]°	4	1.58E-05		1.58E-05			
21.45	11*d* [7/2]°	3	1.30E-05		1.30E-05			

a) Ref. 22. $\sum_l A_{ul}$ is the Einstein coefficient for spontaneous emission.

Table 2. Total relative formation rate constants and electronic-state distribution of Ne* in the $Ne^+/2e^-$ CRR reaction at thermal energy.

State	Number of sublevel	$\sum_u k_0(u)$ (%)	$\sum_u N(u)$ (%)
4*s*	2	16.1	17.0
4*s′*	2	60.6	40.3
3*d*	8	12.8	13.1
3*d′*	4	5.6	6.0
5*s*	2	0.2	0.5
5*s′*	2	0.4	0.6
4*d*	7	0.8	1.7
4*d′*	3	0.4	0.9
6*s*	2	0.07	0.04
5*d*	5	2.7	18.5
5*d′*	2	0.1	1.2
7*s*	2	0.01	
6*d*	2	0.02	
6*d′*	3	0.2	
7*d*	3	0.03	
9*d*	1	0.001	
10*d*	1	0.001	
11*d*	1	0.001	

direct formation and radiative cascade participate in the production of all 4*s* and 4*s′* levels and three 3*d* levels. Many other levels are formed only directly.

In Table 2 are summarized total relative formation rate constants and electronic-state distribution of Ne* produced through the direct $Ne^+/2e^-$ CRR reaction at thermal energy. We found that fifty-two states involving each sublevel are directly formed in the $Ne^+/2e^-$ CRR reaction. The formation of 4*d* levels is consistent with the previous report of Sauter et al.[10] Although Gordeev et al.[11] reported 4*p* levels are formed by the $Ne^+/2e^-$ CRR reaction, we found that they are not formed directly but all of 4*p* levels are produced by radiative cascade from upper levels.

Based on the present data shown in Table 2, major product Ne* states ($\sum_u k_0(u)$ and $\sum_u N(u)$) excluding radiative cascade are 4*s*, 4*s′*, 3*d*, 3*d′*, and 5*d* states, which occupy 16.1, 60.6, 12.8, 5.6, and 2.7% of $\sum_u k_0(u)$ and 17.0, 40.3, 13.1, 6.0, and 18.5% of $\sum_u N(u)$, respectively.

Initial electronic-state distribution formed by direct excitation, $N(u)$, was determined for low energy levels in the 18.38–21.11 eV range, because A_{ul} values are unknown for high energy levels in the 21.14–21.45 eV region.

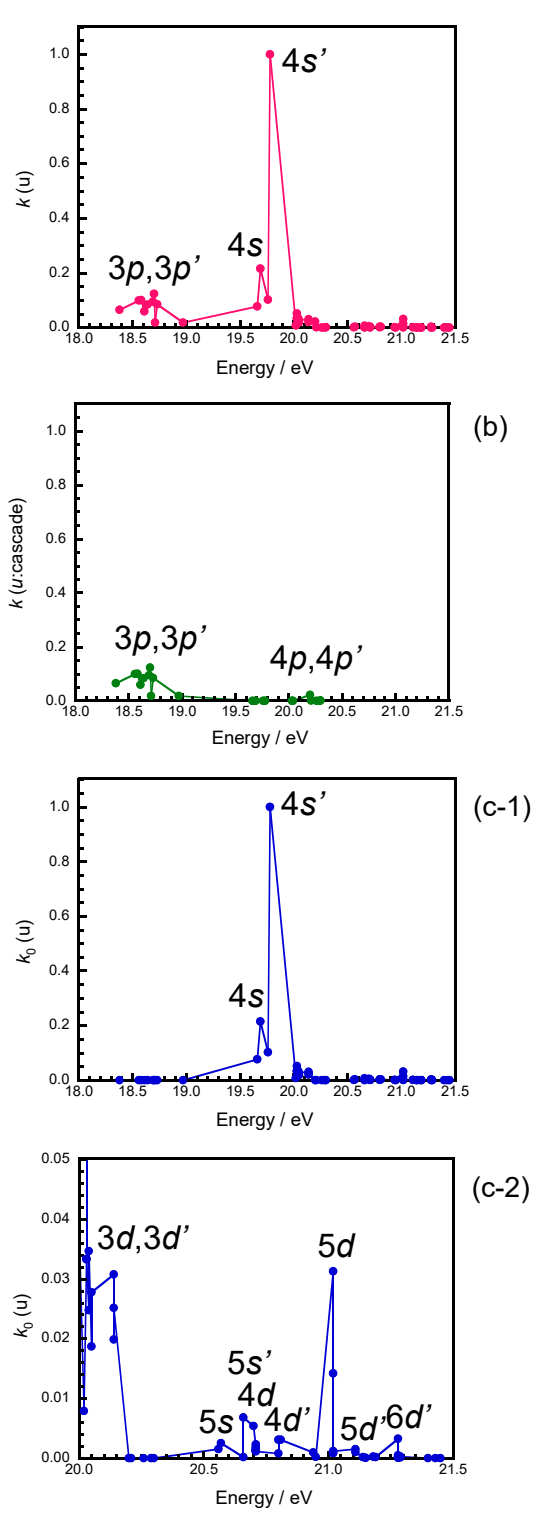

Fig. 3. Dependence of relative formation rate constants on the exciation energy of Ne* in the $Ne^+/2e^-$ CRR reaction: (a) including radiative cascade, (b) radiative cascade, and (c) excluding radiative cascade. (c-2) is expanded data of (c-1) in the 20.0–21.5 eV region.

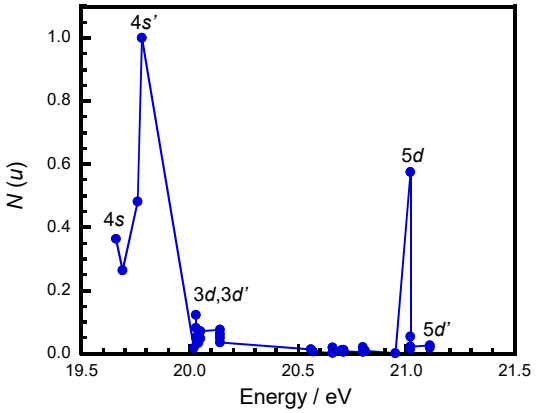

Fig. 4. Electronic-state distributions of Ne* in the $Ne^+/2e^-$ CRR reaction.

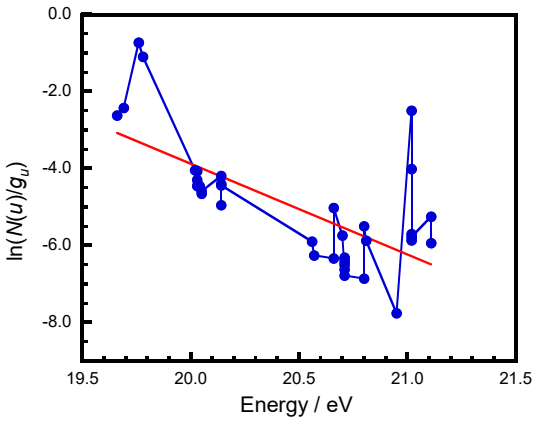

Fig. 5. $\ln(N(u)/g_u)$ vs excitation energy of Ne* in the $Ne^+/2e^-$ CRR reaction.

When $k_0(u)$ values are zero, their $N(u)$ values become also zero. We show only non-zero $N(u)$ states in Table 1 and Fig. 4. Results shown in Table 1 and Fig. 4 indicate that favorable states are $4s$, $4s'$, $3d$, and $3d'$ states in the 19.66–20.14 eV region and the $5d$ states at 21.02 eV.

According to statistic theory, the electronic-state distribution of Ne* formed by CRR reaction (4) may be explained in terms of the Saha equation:

$$N_u = N^+ N_e (g_u/g_e g_i)\,(2\pi mkT/h^2)^{-3/2} \exp(-E_u/kT) \quad (15)$$

where N^+ and N_e are ion and electron densities, g_e and g_i are the statistical weights of a free electron and an Ne^+ ion, and E_u is the energy of Ne*, respectively; a thermal equilibrium between Ne* and free electrons is assumed. If such a Boltzmann equilibrium is established, N_u is given in the form:

$$N(u) = g_u \exp(-E_u/kT) \quad (16)$$

The dependence of $\ln(N(u)/g_u)$ vs E_u was fitted by a straight line, as shown in Fig. 5. From the slope of the straight line, a Boltzmann temperature of 0.43 eV was obtained. This value is close to 0.46 eV observed for the low energy component (22.7–24.4 eV) of He* in the $He^+/2e^-$ CRR,[8] whereas it is lower than 0.54 eV of Ar* in the $Ar^+/2e^-$ CRR.[9]

The $\sum_u k_0(u)$ and $\sum_u N(u)$ values of the product states having the $Ne^+(^2P_{3/2})$ ion core and the $Ne^+(^2P_{1/2})$ ion core are 33:67% and 51:49% respectively. In our previous study on the $Ar^+(^2P_{3/2})/2e^-$ CRR,[9] we discussed the conservation of ion core of $Ar^+(^2P_{3/2})$ in terms of one-electron process and two-electron processes. Since both $^2P_{3/2}$ and $^2P_{1/2}$ spin-orbit components of Ne^+ exist in the present experiment and their relative concentration is not determined. Therefore, it is difficult to discuss the relative contribution of the $Ne^+(^2P_{3/2})/2e^-$ and $Ne^+(^2P_{1/2})/2e^-$ CRR and conservation of ion-core configuration during the CRR reaction. Further detailed experimental study will be required to obtain information on ion-core conservation by separating two spin-orbit components.

4. Summary and Conclusion

148 Ne* lines were observed in the $Ne^+/2e^-$ CRR by using He afterglow. Relative formation rates, $k(u)$, and the electronic-state distribution, $N(u)$, of Ne* in the $Ne^+/2e^-$ CRR were determined in the He flowing afterglow by observing Ne* emissions in the 260–970 nm region. Sixty-eight ns(n=4–7), ns'(n=4 and 5), np(n=3 and 4), np'(n=3 and 4), nd(n=3–7, 9–11), and nd' (n=3–6) levels were identified. Major product Ne* states ($\sum_u k_0(u)$ and $\sum_u N(u)$) excluding radiative cascade were 4*s*, 4*s'*, 3*d*, 3*d'*, and 5*d* states, which occupied 16.1, 60.6, 12.8, 5.6, and 2.7% of $\sum_u k_0(u)$ and 17.0, 40.3, 13.1, 6.0, and 18.5% of $\sum_u N(u)$, respectively. The formation of 4*d* levels is consistent with the previous report of Sauter et al.[10] Although Gordeev et al.[11] reported 4*p* levels are formed by the $Ne^+/2e^-$ CRR, we found that all of them are produced by radiative cascade from upper levels.

The electronic-state distribution of Ne* increased with decreasing excitation energy of Ne*. It was expressed by a single Boltzmann distribution with an effective electronic temperature of 0.43 eV. This value was close to that of He* in the $He^+/2e^-$ CRR (0.46 eV), whereas it was lower than that of Ar* in the $Ar^+/2e^-$ CRR (0.46 eV).

Acknowledgments

The authors acknowledge financial support from the Mitsubishi foundation (1996) and Kyushu University Interdisciplinary Programs in Education and Projects in Research Development (2001–2002). They also give thanks to Prof. Kenji Furuya for his careful reading of our manuscript.

References

1) D. R. Bates, A. E. Kingston, and R. W. P. McWhirter, *Proc. R. Soc., Ser. A*, 267, 297 (1962).
2) J. Stevefelt, J. Boulmer, and J.-F. Delpech, *Phys. Rev. A*, 12, 1246 (1975).
3) C. J. Chen, *J. Chem. Phys.*, 50, 1560 (1969).
4) G. E. Veatch, H. J. Oskam, *Phys. Rev. A*, 1, 1498 (1970).
5) M. R. Flanney, *Adv. Atomic, Mol. Opt. Phys.*, 32, 117 (1994).
6) M. P. Skrzypkowski, R. Johnsen, R. E. Rosati, and M. F. Golde, *Chem. Phys.*, 296, 23 (2004).
7) M. Nakamura, M. Tsuji, M. Tanaka, and Y. Nishimura, *Chem. Lett.*, 25, 279 (1996)
8) M. Tsuji, M. Nakamura, E. Oda, M. Hisano, and Y. Nishimura, *Jpn. J. Appl. Phys.*, 37, 5775 (1998).
9) M. Tsuji, T. Matsuzaki, and T. Tsuji, *Chem. Phys.*, 285, 335 (2002).
10) G. F. Sauter, R. A. Gerber, and H. J. Oskam, *Physica*, 32, 1921 (1966).
11) S. V. Gordeev, V. A. Ivanov, and Yu. E. Skoblo, *Opt. Spectrosc.,* 127, 418 (2019).
12) M. Tsuji, M. Hisano, T. Tanoue, and Y. Nishimura, *Jpn. J. Appl. Phys.*, 39, 4970 (2000).
13) H. Sekiya, M. Tsuji, and Y. Nishimura *Chem. Phys. Lett.*, 100, 494 (1983).
14) H. Obase, M. Tsuji, and Y. Nishimura *Chem. Phys. Lett.*, 105, 214 (1984).
15) M. Tsuji, "*Techniques of Chemistry: Techniques for the Study of Ion Molecule Reactions; Chapter IX. Spectroscopic Probes*", Edited by J. M. Farrar and W. Saunders, Jr., John Wiley & Sons, Inc, Publishers, 489 (1988).
16) A. P. Vitols and H. J. Oskam, *Phys. Rev. A*, 5, 2618 (1972).
17) V. G. Anicich, "*An Index of the Literature for Bimolecular Gas Phase Cation-Molecule Reaction Kinetics*", JPL Publication, 03-19 NASA (2003), and references therein.
18) A. L. Schmeltekoph and F. C. Fehsenfeld, *J. Chem. Phys.*, 53, 3173 (1974).
19) M. Tsuji, E. Oda, M. Tanaka, M. Nakamura, and Y. Nishimura, *Chem. Lett.*, 26, 465 (1997).
20) S. Yamaguchi, M. Tsuji, and Y. Nishimura, *J. Chem. Phys.*, 88, 3111 (1988).
21) A. R. Striganov and N. S. Sventitskii "*Tables of Spectral Lines of Neutral and Ionized Atoms*", Plenum Press, New York, (1979).
22) *Atomic Spectra Database*, *NIST Standard Reference Database*, 78, Ver. 5.9. Oct. (2021).
23) C. E. Moore, "*Atomic Energy Levels*", U.S. GPO, Washington D.C., Natl. Bur. Stand. (U.S.) Circ. 467 (1949).